




Initial-induced coexisting and synchronous firing activities in memristor synapse-coupled Morris–Lecar bi-neuron network

Bocheng Bao · Qinfeng Yang · Dong Zhu · Yunzhen Zhang · Quan Xu · Mo Chen 

Received: 3 October 2019 / Accepted: 23 November 2019 / Published online: 6 December 2019
© Springer Nature B.V. 2019

Abstract A memristor synapse with threshold memductance is employed to couple two neurons for representation of the electromagnetic induction effect triggered by their membrane potential difference. This paper presents a memristor synapse-coupled bi-neuron network by bidirectionally coupling two three-dimensional heterogeneous or homogeneous Morris–Lecar neurons with such a memristor synapse. The memristive bi-neuron network possesses a line equilibrium set with its stability related to the induction coefficient and memristor initial value. Coexisting firing activities in the heterogeneous memristive bi-neuron network are explored using bifurcation plots, phase plots, and time sequences, upon which the initial-induced infinitely many firing patterns including hyperchaotic, chaotic, and periodic bursting and tonic-spiking patterns are disclosed, indicating the emergence of the initial-induced extreme multistability. Furthermore, synchronous firing activities in homogeneous memristive bi-neuron network are investigated using the time sequences, synchronization transition states, and mean synchronized errors. The results demonstrate that the synchronous firing activities are associated with the induction coefficient and specially

associated with the initial values of memristor synapse and coupling neurons. Finally, an FPGA-based electronic bi-neuron network is designed to experimentally confirm the memristor initial-induced coexisting firing activities.

Keywords Memristor synapse · Bi-neuron network · Initial value · Coexisting activity · Synchronous activity

1 Introduction

Based on the proposed numerous mathematical models, the essential electrical activities, basic neuron dynamics including resting, tonic-spiking, and bursting behaviors, of biological neurons have been revealed by carrying out bifurcation analyses in the past few years. In electrophysiological environments, the neuron electrical activities could be influenced by electromagnetic radiation [1]. From the point of view of electromagnetic induction theory, the magnetic flux could be employed to describe the electromagnetic radiation effect [2–6] and the flux-controlled memristor could be taken as the coupled synapse between the neuronal cells [7–10]. To date, some memristor-based neuron models with the electromagnetic induction effects have been proposed [7–15], from which the abundant firing activities have been disclosed, such as synchronous firing activities [7–10], mode transition and selection

B. Bao · Q. Yang · D. Zhu · Q. Xu · M. Chen (✉)
School of Information Science and Engineering,
Changzhou University, Changzhou 213164, China
e-mail: mchen@cczu.edu.cn

Y. Zhang
Department of Electronic Engineering, Nanjing University of
Science and Technology, Nanjing 210094, China

between tonic-spiking and bursting [11–13], coherence resonance of the spiking regularity [14], and coexisting multiple firing patterns [15–17]. When different firing activities appear in neurons, the differences of neuron membrane potentials can give birth to the electromagnetic induction effects [17], behaving like memristor synapses for coupling these neurons. Consequently, two neurons can be regarded as a memristor synapse-coupled neural network [10, 17], in which the memristor synapse plays a key role in the information propagation and regulation mechanism of these neurons.

Initial-dependent multi-stable firing patterns were affirmed by actual experimental evidences [18]. Recently, Kim and Jones [19] investigated the dynamical effect of asymmetric electrotonic coupling and thereby uncovered the phenomenon of bistability in a two-compartment model. On the basis of the two- and three-dimensional Hindmarsh–Rose neuron models [15, 20], the author of this paper discussed the hidden coexisting asymmetric behaviors caused by memristive electromagnetic induction current and coexisting asymmetric bursters induced by the external AC stimulus in single neuron. Meanwhile, on the basis of the three-dimensional Morris–Lecar neuron model, the author of this paper [21] explored the chaotic bursting dynamics and coexisting multi-stable firing patterns also. In contrast, Pisarchik et al. [22] investigated the asymmetry induced multistability in the coupled neuronal oscillators based on the three-dimensional Hindmarsh–Rose neuron model. Furthermore, Bao et al. [23] reported the infinitely many coexisting firing patterns with hidden extreme multistability in an improved non-autonomous memristive FitzHugh–Nagumo circuit. The initial-dependent multistability or extreme multistability not only allows nonlinear dynamical system to possess great flexibility for potential applications [24], but also promotes new challenges for controlling of multiple stable states [25, 26]. The authors noticed that the coexistence of infinitely many disconnected attractors, also known as extreme multistability, was primitively reported in the unidirectionally coupled Lorenz systems [27], bidirectionally coupled Rössler oscillators [28], and bidirectionally memristor-coupled system [29] due to the appearance of incomplete synchronization. The problem that remains is whether the coexistence of infinitely many disconnected firing patterns also emerges in a memristor synapse-coupled neural network and how the ini-

tial values of memristor synapse and coupling neurons induce the extreme multistability. With these considerations, this paper considers a Morris–Lecar bi-neuron network coupled by a bidirectional memristor synapse and then studies its coexisting firing activities with extreme multistability in the heterogeneous case, which has not been revealed yet in the previously reported literature. Therefore, such an initial-dependent extreme multistability is an innovative point of our manuscript.

It is all known that abundant collective behaviors appear in the actual neural system due to the interactions in neurons [30–35], among them synchronization is the outstanding collective features in neuroscience [36], which is regarded as one of the mechanisms to propagate and to code information in brain [37, 38]. However, there are different kinds of brain disorder diseases, such as Alzheimer’s, epilepsy, Parkinson’s, and schizophrenia, which are involved with the abnormal activities of synchronization [39]. Therefore, neuron synchrony is a fundamental topic in neuroscience. For this reason, this paper also considers the synchronous firing activities of the proposed memristor synapse-coupled Morris–Lecar bi-neuron network in the homogeneous case, which could provide new insights for the synchronization collective behaviors [40], especially induced by the initial values of memristor synapse and coupling neurons. Additionally, the digitally circuit-implemented electronic neurons and their constructing neuronal networks can mimic the single neuron firing activities and synchronous firing activities [21, 41–43], which could effectively promote the integrated circuit (IC) design and artificial intelligence applications of cellular neural networks [44].

The rest is arranged as follows. In Sect. 2, a Morris–Lecar bi-neuron network bidirectionally coupled by a memristor synapse is presented and the stability for its line equilibrium set is analyzed. In Sect. 3, coexisting firing activities in the heterogeneous memristive bi-neuron network are explored using numerical plots, upon which initial-induced infinitely many firing patterns, i.e., extreme multistability, are disclosed. The following Sect. 4 investigates synchronous firing activities in the homogeneous memristive bi-neuron network theoretically and numerically. Moreover, an FPGA-based electronic neuronal network is designed and the corresponding experimental observations are performed to confirm the numer-

ical plots in Sect. 5. Finally, it is a conclusion of this paper.

2 Memristor synapse-coupled Morris–Lecar bi-neuron network

Consider a memristor synapse to couple two neurons for representation of the electromagnetic induction effect triggered by their membrane potential difference. For the inducted current I_M and membrane potential difference $V_M = V_1 - V_2$, the characterized memristor synapse can be described by

$$I_M = W(\varphi)V_M = \tanh(\varphi)(V_1 - V_2)$$

$$\dot{\varphi} = V_M = V_1 - V_2 \quad (1)$$

where φ is an inner flux state variable triggered by the membrane potential difference of two coupling neurons and $W(\varphi) = \tanh(\varphi)$ is a threshold memductance [16,23]. Note that the memristor synapse model is an ideal flux-controlled memristor, distinguishing from the non-ideal flux-controlled memristor employed in [17].

A three-dimensional fast-slow autonomous Morris–Lecar neuron model was reported by [21,45–47], which can be employed to characterize membrane potential firing activities in biological neurons. Based on the model of memristor synapse in (1), a memristor synapse-coupled Morris–Lecar bi-neuron network, also abbreviated as memristive bi-neuron network, is derived, which is expressed as

$$\begin{aligned} \dot{V}_1 &= g_{Ca}M_{\infty 1}(V_{Ca} - V_1) + g_K W_1(V_{K1} - V_1) \\ &\quad + g_L(V_L - V_1) - I_1 + kI_M \\ \dot{W}_1 &= \tau_{W1}(W_{\infty 1} - W_1) \\ \dot{I}_1 &= \varepsilon(V_0 + V_1) \\ \dot{V}_2 &= g_{Ca}M_{\infty 2}(V_{Ca} - V_2) + g_K W_2(V_{K2} - V_2) \\ &\quad + g_L(V_L - V_2) - I_2 - kI_M \\ \dot{W}_2 &= \tau_{W2}(W_{\infty 2} - W_2) \\ \dot{I}_2 &= \varepsilon(V_0 + V_2) \\ \dot{\varphi} &= V_1 - V_2 \end{aligned} \quad (2)$$

where

$$\begin{aligned} M_{\infty j}(V_j) &= 0.5 + 0.5 \tanh[(V_j - V_a)/V_b] \\ W_{\infty j}(V_j) &= 0.5 + 0.5 \tanh[(V_j - V_c)/V_d] \\ \tau_{Wj}(V_j) &= (1/3) \cosh[0.5(V_j - V_c)/V_d] \end{aligned} \quad (3)$$

The subscripts $j = 1, 2$ stand for the first neuron (also called neuron 1) and second neuron (also called neuron 2) of the two coupling neurons, V_j, W_j are the fast spiking variables and I_j is the slow bursting variable induced by the membrane potential of j th neuron. The induction coefficient k represents the coupling strength of electromagnetic induction between the two neurons. Except for the parameters V_{K1}, V_{K2} , and ε , the other parameters are determined from [21,45] as $V_{Ca} = 1$ mV, $V_L = -0.5$ mV, $g_{Ca} = 1.2$ mS/cm², $g_K = 2$ mS/cm², $g_L = 0.5$ mS/cm², $V_0 = 0.2$ mV, $V_a = -0.01$ mV, $V_b = 0.15$ mV, $V_c = 0.1$ mV, and $V_d = 0.05$ mV. Note that two membrane capacitances are fixed as $1 \mu\text{F}/\text{cm}^2$ for simplicity.

Distinctly, the memristive bi-neuron network (2) owns a line equilibrium set, which can be expressed as

$$P = (-V_0, \bar{W}_{\infty}, \bar{I}_1, -V_0, \bar{W}_{\infty}, \bar{I}_2, \mu) \quad (4)$$

where μ is an uncertain constant associated with the memristor initial position,

$$\begin{aligned} \bar{M}_{\infty}(V_0) &= 0.5 - 0.5 \tanh[(V_0 + V_a)/V_b] \\ \bar{W}_{\infty}(V_0) &= 0.5 - 0.5 \tanh[(V_0 + V_c)/V_d] \\ \bar{\tau}_W(V_0) &= (1/3) \cosh[0.5(V_0 + V_c)/V_d] \end{aligned} \quad (5)$$

and

$$\begin{aligned} \bar{I}_1 &= g_{Ca}\bar{M}_{\infty}(V_{Ca} - V_0) + g_K\bar{W}_{\infty}(V_{K1} - V_0) \\ &\quad + g_L(V_L - V_0) \\ \bar{I}_2 &= g_{Ca}\bar{M}_{\infty}(V_{Ca} - V_0) + g_K\bar{W}_{\infty}(V_{K2} - V_0) \\ &\quad + g_L(V_L - V_0) \end{aligned} \quad (6)$$

Therefore, the line equilibrium set (4) is independent of the induction coefficient k , but closely dependent on the memristor initial position μ .

With (2), (3), (4), and (5), the Jacobian matrix for the memristive bi-neuron network at P is deduced as

$$\mathbf{J} = \begin{bmatrix} -H_1 & g_K(V_{K1} + V_0) & -1 & -k \tanh(\mu) & 0 & 0 & 0 \\ H_2 & -\bar{\tau}_W & 0 & 0 & 0 & 0 & 0 \\ \varepsilon & 0 & 0 & 0 & 0 & 0 & 0 \\ -k \tanh(\mu) & 0 & 0 & -H_1 & g_K(V_{K2} + V_0) & -1 & 0 \\ 0 & 0 & 0 & H_2 & -\bar{\tau}_W & 0 & 0 \\ 0 & 0 & 0 & \varepsilon & 0 & 0 & 0 \\ 1 & 0 & 0 & -1 & 0 & 0 & 0 \end{bmatrix} \tag{7}$$

where

$$\begin{aligned}
 H_1 &= g_{Ca} \bar{M}_\infty + g_K \bar{W}_\infty + g_L + k \tanh(\mu) \\
 &\quad - 0.5 g_{Ca} V_b^{-1} (V_{Ca} + V_0) \operatorname{sech}^2[(V_0 + V_a)/V_b] \\
 H_2 &= 0.5 \bar{\tau}_W V_d^{-1} \operatorname{sech}^2[(V_0 + V_c)/V_d]
 \end{aligned}$$

Thus, the stability of the line equilibrium set (4) is related to the induction coefficient k and memristor initial position μ .

With (7), the eigenvalues at P can be numerically calculated in the considered regions of $k \in [0, 1]$ and $\mu \in [-10, 10]$. When $V_{K1} = V_{K2} = -0.7$ mV and $\varepsilon = 0.005$, the eigenvalues have one zero root, four (or two) positive roots, and two (or four) negative roots, indicating that every point in the line equilibrium set P is a critical saddle point. When $V_{K1} = V_{K2} = -410$ mV and $\varepsilon = 0.1$, the eigenvalues have one zero root, one pair (or two pairs) of complex roots with positive real parts, and four negative roots (or two negative roots and one pair of complex roots with negative real parts), implying that every point in the line equilibrium set P is a critical saddle-focus. In contrast, when $V_{K1} = -410$ mV, $V_{K2} = -0.7$ mV, and $\varepsilon = 0.1$, the eigenvalues have the same roots as those for $V_{K1} = V_{K2} = -410$ mV and $\varepsilon = 0.1$, i.e., every point in the line equilibrium set P is a critical saddle-focus.

3 Coexisting firing activities in heterogeneous memristive bi-neuron network

The voltage V_K in the potassium ion-channel of neuron is a variable parameter [47]. When two different parameters of V_K are employed, two typical fold/Hopf and fold/homoclinic bursting patterns can be revealed in the three-dimensional autonomous Morris–Lecar neuron model [21, 47]. Denote $V_{K1} = -410$ mV for neuron 1 and $V_{K2} = -0.7$ mV for neuron 2 along with $\varepsilon = 0.1$. As a result, the parameters between the two coupling neurons are inconsistent, indicating that the

memristor synapse-coupled Morris–Lecar bi-neuron network is heterogeneous. For this case, we focus on the initial-induced coexisting firing activities in the heterogeneous memristive bi-neuron network. Note that MATLAB ODE23s algorithm with the time-step 0.01 and ODE23s-based Wolf’s Jacobian matrix method is used for simulations of two and one dimension of bifurcation diagrams and Lyapunov exponents (LEs).

The bi-neuron initial values are fixed as (0.01 mV, 0, 0, -0.01 mV, 0, 0) and the memristor initial value φ_0 and induction coefficient k are adjusted in the regions [-2 mWb, 4 mWb] and [0.02, 0.4], respectively. When both φ_0 and k are continuously changed in their regions, two dimensions of bifurcation plots in the $\varphi_0 - k$ plane are depicted in Fig. 1. The two dimensions of bifurcation diagram in Fig. 1a are painted with different colors through detecting the periodicities of the slow bursting variable I_1 of neuron 1. The red regions are coded by CH for representing chaotic bursting patterns when the periodicities are greater than 4 and the magenta, brown, dark green, and blue regions are respectively coded by P4, P3, P2, and P1 for representing periodic bursting patterns with different bursters. In contrast, the two dimension of dynamical map in Fig. 1b is painted with different colors through calculating the values of the largest LE [48]. The yellow-red-white regions with positive largest LE stand for chaotic bursting patterns and the dark-yellow regions with zero largest LE stand for periodic bursting patterns. Observed from Fig. 1a, b, it is sure that the firing activities described by the two dimension of bifurcation diagram coincide with those described by the two dimension of dynamical map.

Take the induction coefficient $k = 0.07$ and 0.2 as cases to further explore the memristor initial-induced dynamical behaviors in the heterogeneous memristive bi-neuron network. When the memristor initial value φ_0 is increased from -2 mWb to 4 mWb, the bifurcation diagram of the maxima $I_{1,max}$ of the slow bursting variable I_1 of neuron 1 and the corresponding first three finite-time LEs are given, as shown in Fig. 2, in

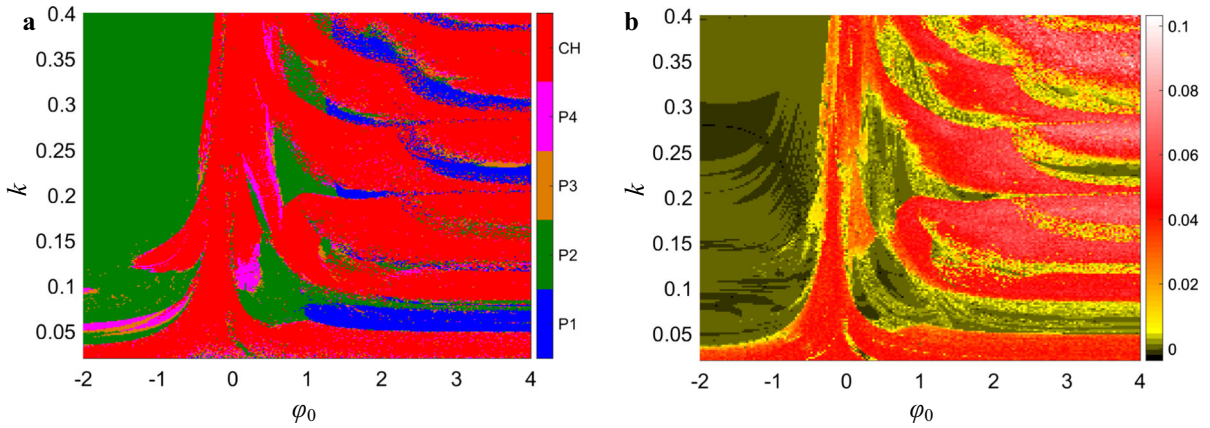


Fig. 1 Two dimension of the mixed initial value and parameter-related bifurcation plots in the $\varphi_0 - k$ plane with the bi-neuron initial values (0.01 mV, 0, 0, -0.01 mV, 0, 0), where the unit of

φ_0 is mWb **a** bifurcation diagram depicted by the periodicities of the slow bursting variable I_1 of neuron 1 **b** dynamical map depicted by the values of the largest LE

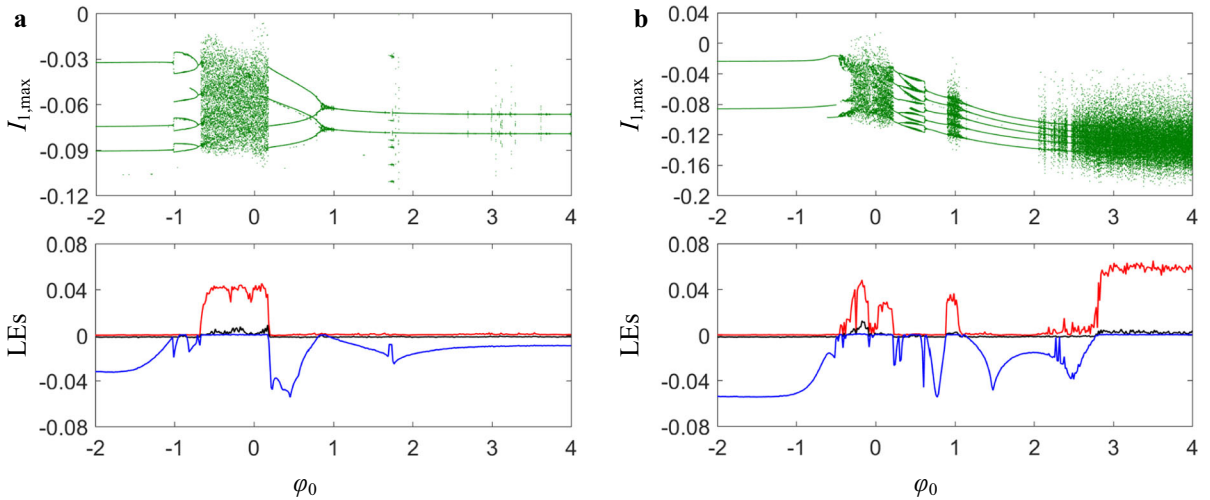


Fig. 2 One dimension of the bifurcation behaviors induced by the initial value φ_0 of memristor, bifurcation diagram of the maxima $I_{1,max}$ of the slow bursting variable I_1 of neuron 1 (top) and

corresponding first three LEs (bottom), where the unit of φ_0 is mWb **a** bifurcation behaviors for $k = 0.07$ **b** bifurcation behaviors for $k = 0.2$

which the dynamical behaviors depicted by the bifurcation diagrams do well match with those depicted by the finite-time LEs. The numerical plots manifest that there exist complex memristor initial-dependent dynamical behaviors in the heterogeneous memristive bi-neuron network, indicating the emergence of the memristor initial-induced extreme multistability. Such an initial-dependent extreme multistability has not been found yet in the previously reported memristor synapse-coupled neuron networks. Only multistability with up

to four types of coexisting patterns has been uncovered in a five-dimensional memristor-coupled Hindmarsh–Rose neuron model [17] or a three-dimensional memristor synapse-coupled Hopfield neural network with two neurons [48].

In the first case of Fig. 2a, the induction coefficient is fixed as $k = 0.07$. In the heterogeneous memristive bi-neuron network, the action potential starts from a periodic burster-4 bursting for neuron 1 at $\varphi_0 = -2$ mWb and breaks into a periodic bursting with double burster-

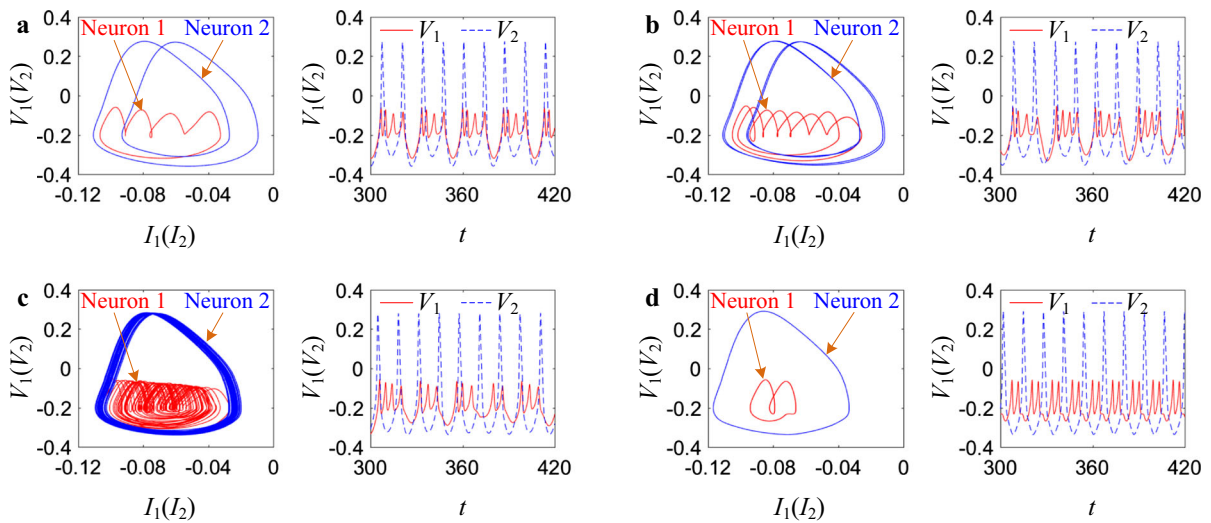


Fig. 3 Memristor initial-induced infinitely many coexisting patterns for $k = 0.07$, the lefts are phase plots of neuron 1 in the $I_1 - V_1$ plane and neuron 2 in the $I_2 - V_2$ plane, the rights are time sequences of the membrane potentials V_1 and V_2 , where the units of V_1, V_2 are mV and the units of I_1, I_2 are μA **a**

4 at $\varphi_0 = -1.02$ mWb. The periodic double burster-4 bursting gradually evolves into the periodic burster-4 bursting and then jumps into a hyperchaotic bursting with disordered spikes at $\varphi_0 = -0.68$ mWb through chaos crisis. The hyperchaotic bursting sustains to $\varphi_0 = 0.18$ mWb, after which another periodic burster-4 bursting with different structures comes again via tangent bifurcation route. Finally, the periodic burster-4 bursting degrades into a periodic burster-2 bursting at $\varphi_0 = 0.94$ mWb via reverse period-doubling bifurcation route. For four specified values of the memristor initial value φ_0 , the memristor initial-induced infinitely many coexisting firing patterns are shown in Fig. 3, where the phase plots of two neurons and time sequences of two membrane potentials are simulated concurrently.

In the second case of Fig. 2b, the induction coefficient is changed as $k = 0.2$. In the heterogeneous memristive bi-neuron network, the action potential begins with a periodic burster-5 bursting for neuron 1 at $\varphi_0 = -2$ mWb and mutates into a chaotic bursting with variable burster at $\varphi_0 = -0.46$ mWb through the continuous deformation of the periodic burster. The chaotic bursting evolves into a hyperchaotic bursting and further breaks into another periodic burster-5 bursting with different structures at $\varphi_0 = 0.22$ mWb via tangent bifurcation route. Another periodic burster-5 bursting gradually splits into a periodic quadruple burster-5 burst-

ing via reverse period-doubling bifurcation route and then unites into the periodic burster-5 bursting at $\varphi_0 = 0.63$ mWb. As φ_0 increases further, the chaotic bursting appears again at $\varphi_0 = 0.90$ mWb and ends at $\varphi_0 = 1.05$ mWb. Afterward, the periodic burster-5 bursting lasts a long initial value region, and then enters into the chaotic bursting, and finally settles on the hyperchaotic bursting. Similarly, for six specified values of the memristor initial value φ_0 , the phase plots and time sequences of the induced infinitely many coexisting firing patterns are shown in Fig. 4, in which the phase plots of two neurons and time sequences of two membrane potentials are simulated concurrently. Besides, it is clearly seen that the periodic burster-5 bursting in Fig. 4c has different pattern structure from that in Fig. 4a, whereas the hyperchaotic bursting in Fig. 4f possesses a distinguishing pattern structure from that in Fig. 4b, implying the coexistence of different kinds of firing patterns.

Note that for the hyperchaotic bursting and hyperchaotic tonic-spiking shown in Figs. 3c, 4b, and 4f, the first three finite-time LEs are calculated as (0.0448, 0.0042, 0.0001), (0.0435, 0.0098, 0.0001), and (0.0578, 0.0036, 0.0000), respectively, indicating the appearance of hyperchaotic firing activities in the heterogeneous memristive bi-neuron network.

To conveniently explore dynamical effects of the bi-neuron initial values on the heterogeneous memristive

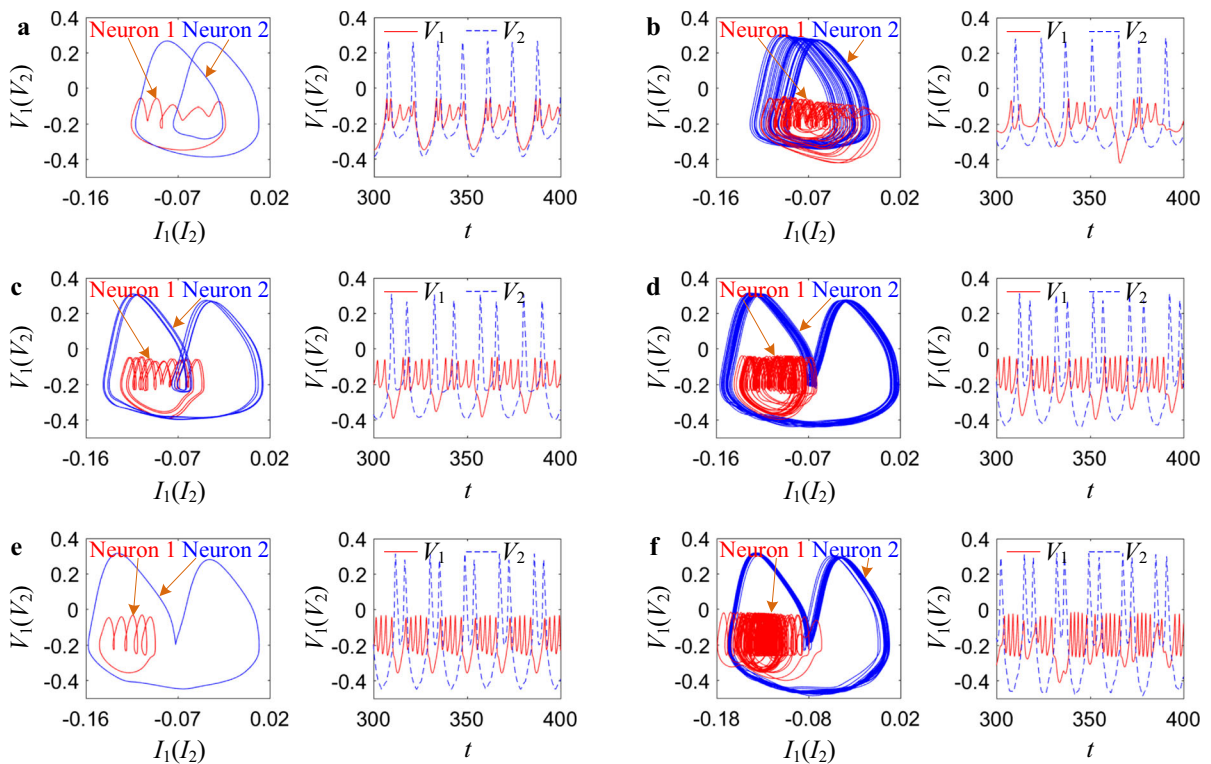


Fig. 4 Memristor initial-induced infinitely many coexisting patterns for $k = 0.2$, the lefts are phase plots of neuron 1 in the $I_1 - V_1$ plane and neuron 2 in the $I_2 - V_2$ plane, the rights are time sequences of the membrane potentials V_1 and V_2 , where the units of V_1, V_2 are mV and the units of I_1, I_2 are μA **a** periodic burster-5 bursting and periodic tonic-spiking for $\varphi_0 = -1 \text{ mWb}$ **b** hyperchaotic bursting and hyperchaotic tonic-spiking for φ_0

$= -0.15 \text{ mWb}$ **c** periodic bursting with quadruple burster-5 and periodic tonic-spiking for $\varphi_0 = 0.45 \text{ mWb}$ **d** chaotic bursting and chaotic tonic-spiking for $\varphi_0 = 1 \text{ mWb}$ **e** another periodic burster-5 bursting and periodic tonic-spiking for $\varphi_0 = 1.5 \text{ mWb}$ **f** hyperchaotic bursting and hyperchaotic tonic-spiking for $\varphi_0 = 3 \text{ mWb}$

bi-neuron network, the induction coefficient and memristor initial value are kept unchanged as $k = 0.2$ and $\varphi_0 = 0$ respectively. The bi-neuron initial values are considered as $(0.01 \text{ mV}, 0, I_{10}, -0.01 \text{ mV}, 0, I_{20})$, in which both the measurable initial values I_{10} and I_{20} are varied in the regions $[-0.2 \mu\text{A}, 0.2 \mu\text{A}]$. The basin of attraction in the $I_{10}-I_{20}$ plane is shown in Fig. 5a, which demonstrates that different topologically chaotic (red and magenta) and periodic (blue, cyan, green, and orange) bursting firings coexisted in the heterogeneous memristive bi-neuron network. Corresponding to the initial values appeared in different attracting regions of Fig. 5a, phase plots of the chaotic and periodic bursting firings are together drawn in Fig. 5b. Note that only four types of periodic bursting firings labeled by PI - PV and two types of chaotic bursting firings labeled by CI, CII are classified in Fig. 5, the other types of peri-

odic and chaotic bursting firings with other different positions are not provided. Consequently, the bi-neuron initial values can also trigger complex firing activities coexisted in the heterogeneous memristive bi-neuron network.

4 Synchronous firing activities in homogeneous memristive bi-neuron network

The parameters of two coupling neurons are employed as $V_{Ca} = 1 \text{ mV}$, $V_L = -0.5 \text{ mV}$, $g_{Ca} = 1.2 \text{ mS/cm}^2$, $g_K = 2 \text{ mS/cm}^2$, $g_L = 0.5 \text{ mS/cm}^2$, $V_0 = 0.2 \text{ mV}$, $V_a = -0.01 \text{ mV}$, $V_b = 0.15 \text{ mV}$, $V_c = 0.1 \text{ mV}$, $V_d = 0.05 \text{ mV}$, $V_{K1} = V_{K2} = V_K = -410 \text{ mV}$, and $\varepsilon = 0.1$. Thus, the two coupling neurons have exactly the same parameters, indicating that the memristive bi-neuron network is homogeneous. Based on this, we focus on the initial-

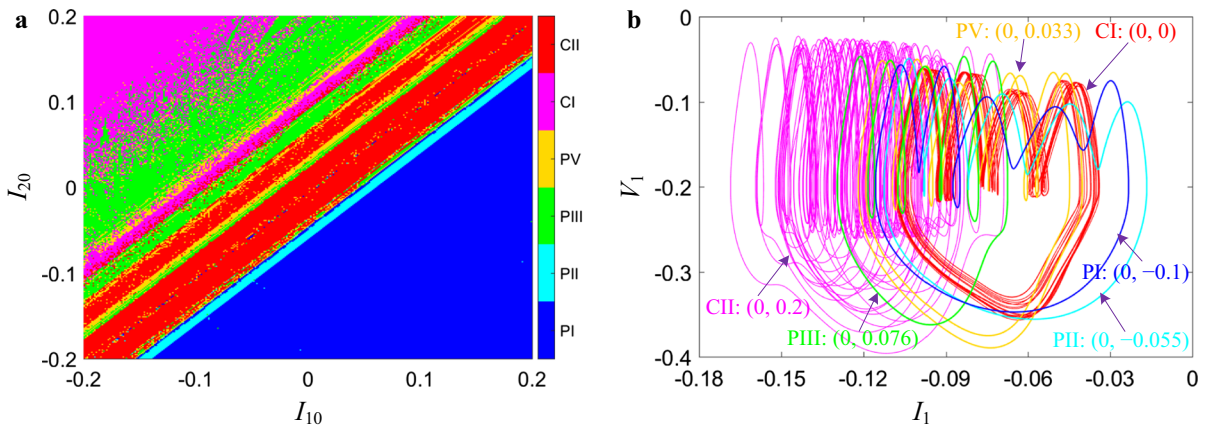


Fig. 5 Coexisting bursting firing behaviors for $k = 0.2$ and $\varphi_0 = 0$ mWb with the bi-neuron initial values $(0.01$ mV, $0, I_{10}, -0.01$ mV, $0, I_{20})$, where the units of V_1 and I_1 are mV and μ A respectively **a** basin of attraction in the I_{10} – I_{20} plane **b** coexis-

tence of different topologically chaotic (brown and black) and periodic (blue, red, and green) bursting firings. (Color figure online)

induced synchronous firing activities in the homogeneous memristive bi-neuron network.

4.1 Complete synchronization

Consider a nonlinear dynamical system

$$\dot{x} = h(x) \tag{8}$$

in which $h: D \rightarrow R^n$ represents a continuously differentiable map from a real domain $D \subset R^n$ into R^n and the origin $x = 0$ locates in D .

The following theorem provides conditions under which we can reach conclusion about the stability of the origin as an equilibrium set for the nonlinear dynamical system by inspecting its stability as the equilibrium set for the linear dynamical system [49].

Theorem 1 ([49], Theorem 4.7, p. 139) *Suppose $x = 0$ to be an equilibrium point for the nonlinear dynamical system (8). Let*

$$A = \left. \frac{\partial h(x)}{\partial x} \right|_{x=0} \tag{9}$$

Then, the origin is asymptotically stable if $Re(\lambda_i) < 0$ for all eigenvalues of A .

Denote $e_1 = V_1 - V_2, e_2 = W_1 - W_2, e_3 = I_1 - I_2$, and $e = [e_1, e_2, e_3]^T$. By (2), the error system of the homogeneous memristive bi-neuron network can be described as

$$\begin{aligned} \dot{e}_1 &= 2kI_M - g_L e_1 + g_K V_K e_2 - e_3 + F_1(V_j, W_j, e) \\ \dot{e}_2 &= F_2(V_j, W_j, e) \\ \dot{e}_3 &= \varepsilon e_1 \end{aligned} \tag{10}$$

where

$$\begin{aligned} I_M &= \tanh(\varphi)(V_1 - V_2) = \tanh(\varphi)e_1 \\ F_1(V_j, W_j, e) &= g_{Ca} V_{Ca}(M_{\infty 1} - M_{\infty 2}) \\ &\quad - g_{Ca}(M_{\infty 1} V_1 - M_{\infty 2} V_2) \\ &\quad - g_K(W_1 V_1 - W_2 V_2) \\ F_2(V_j, W_j, e) &= \tau_{W1}(W_{\infty 1} - W_1) - \tau_{W2}(W_{\infty 2} - W_2) \end{aligned}$$

For the sake of ease, the aforementioned parameters of two coupling neurons are utilized directly. Thus, $F_1(V_j, W_j, e)$ and $F_2(V_j, W_j, e)$ can be further simplified as

$$\begin{aligned} F_1(V_j, W_j, e) &= 1.2(M_{\infty 1} - M_{\infty 2}) - 1.2(M_{\infty 1} V_1 \\ &\quad - M_{\infty 2} V_2) - 2(W_1 V_1 - W_2 V_2) \\ &= 0.6\{\tanh[(100V_1 + 1)/15] \\ &\quad - \tanh[(100V_2 + 1)/15]\} \\ &\quad - 0.6\{(V_1 - V_2) + V_1 \tanh[(100V_1 \\ &\quad + 1)/15] - V_2 \tanh[(100V_2 + 1)/15]\} \\ &\quad - 2(W_1 V_1 - W_1 V_2 + W_1 V_2 - W_2 V_2) \\ &= -0.6e_1 - 2W_1 e_1 - 2V_2 e_2 \\ &\quad + 0.6\{\tanh[(100V_1 + 1)/15] \\ &\quad - \tanh[(100V_2 + 1)/15]\} \end{aligned}$$

$$\begin{aligned}
 & -0.6\{V_1 \tanh[(100V_1+1)/15] \\
 & - V_2 \tanh[(100V_2+1)/15]\} \\
 F_2(V_j, W_j, e) = & (\tau_{W1} W_{\infty 1} - \tau_{W2} W_{\infty 2}) - (\tau_{W1} W_1 \\
 & - \tau_{W1} W_2 + \tau_{W1} W_2 - \tau_{W2} W_2) \\
 = & 6^{-1}[\cosh(10V_1-1) \\
 & - \cosh(10V_2-1)] \\
 & + 6^{-1}[\cosh(10V_1-1) \tanh(20V_1-2) \\
 & - \cosh(10V_2-1) \tanh(20V_2-2)] \\
 & - 3^{-1}e_2 \cosh(10V_1-1) \\
 & - 3^{-1}W_2[\cosh(10V_1-1) \\
 & - \cosh(10V_2-1)] \\
 = & -3^{-1}e_2 \cosh(10V_1-1) \\
 & + 6^{-1}[\cosh(10V_1-1) \\
 & - \cosh(10V_2-1)] \\
 & + 6^{-1} \tanh(20V_1-2)[\cosh(10V_1 \\
 & - 1) - \cosh(10V_2-1)] \\
 & + 6^{-1} \cosh(10V_2-1)[\tanh(20V_1 \\
 & - 2) - \tanh(20V_2-2)] \\
 & - 3^{-1}W_2[\cosh(10V_1-1) \\
 & - \cosh(10V_2-1)]
 \end{aligned}$$

It is easy to obtain that the origin $e = \mathbf{0}$ is the equilibrium point for the error system (10). Therefore, we have the following theorem.

Theorem 2 *Set $|W_1| \leq L_0$, if $2L_0 - 2k \tanh(\varphi) + 1.1 > 0$, and $\varepsilon > 0$ the zero solution of the error system (10) is asymptotically stable. Thus, the two coupling neurons in the homogeneous memristive bi-neuron network are complete synchronization.*

Proof As the error system (10) has the equilibrium point $e = \mathbf{0}$. Let us investigate the stability of zero solution by using linearization. From (9), the Jacobian matrix A at the origin is given by

$$A = \begin{bmatrix} 2k \tanh(\varphi) - 1.1 - 2W_1 & 2(V_K - V_2) & -1 \\ 0 & -3^{-1} \cosh(10V_1 - 1) & 0 \\ \varepsilon & 0 & 0 \end{bmatrix} \tag{11}$$

we set $L_1 = 2W_1 - 2k \tanh(\varphi) + 1.1$, $L_2 = 2(V_2 - V_K)$, $L_3 = 3^{-1} \cosh(10V_1 - 1)$, then the Jacobian matrix A can be rewritten as

$$A = \begin{bmatrix} -L_1 & -L_2 & -1 \\ 0 & -L_3 & 0 \\ \varepsilon & 0 & 0 \end{bmatrix} \tag{12}$$

The eigenvalues of A are

$$\begin{aligned}
 \lambda_1 &= -L_3 \\
 \lambda_{2,3} &= -0.5L_1 \pm 0.5\sqrt{L_1^2 - 4\varepsilon}
 \end{aligned} \tag{13}$$

As $\cosh(10V_1 - 1) \geq 1$ is always true, there yields $L_3 > 0$, i.e., the eigenvalue λ_1 satisfies $\lambda_1 < 0$. For $|W_1| \leq L_0$ and $2L_0 - 2k \tanh(\varphi) + 1.1 > 0$, we have $L_1 > 0$. As $\varepsilon > 0$, the eigenvalues $\lambda_{2,3}$ satisfy $\lambda_{2,3} < 0$. Consequently, by Theorem 1, the zero solution of the error system (10) is asymptotically stable. Thus, the two coupling neurons in the homogeneous memristive bi-neuron network are complete synchronization. \square

Remark 1 Noteworthy, from the seventh equation of (2), we have $\varphi = \varphi_0 + \int_0^t e_1 d\tau$, thus the L_1 not only depends on the induction coefficient k and bound of W_1 , but also depends on the memristor initial value φ_0 . Of particular importance, for fixed L_0 , there is the condition $2k \tanh(\varphi) < 2L_0 + 1.1$. When the zero solution is asymptotically stable, there gets $\varphi = \varphi_0 + \int_0^t e_1 d\tau \approx \varphi_0$, indicating that the two coupling neurons are easier to synchronize for more negative memristor initial value along with larger induction coefficient.

Remark 2 What needs special attention is that, in the linearization system $\dot{e} = Ae$, the solution actually satisfies $\|e(t)\| \leq \|e(t_0)\| e^{\max\{Re(\lambda_i)\} \cdot (t-t_0)}$, thus, the stability depends on the initial value $e(t_0)$ and eigenvalue real part $Re(\lambda_i)$. In a short time, the initial value $e(t_0)$ will have great influence on the stability [50], i.e., synchronization of the two coupling neurons. But, in a long time, the $Re(\lambda_i)$ plays a decisive role over the initial value $e(t_0)$. That is, the initial value $e(t_0)$ have influence on synchronization of the two coupling neurons, but with the passage of time, the initial value effect on synchronization gradually decreases and the influence of $Re(\lambda_i)$ on synchronization gradually highlights.

4.2 Numerical validations

Now, we perform the numerical validations for the different collective behaviors, i.e., synchronization in the memristive bi-neuron network (2). The aforementioned parameters for the homogeneous memristive bi-neuron network are kept unchanged.

Firstly, the bi-neuron initial values are fixed as (0.01 mV, 0, 0, -0.01 mV, 0, 0) and both the induction coefficient k and memristor initial value φ_0 are tunable.

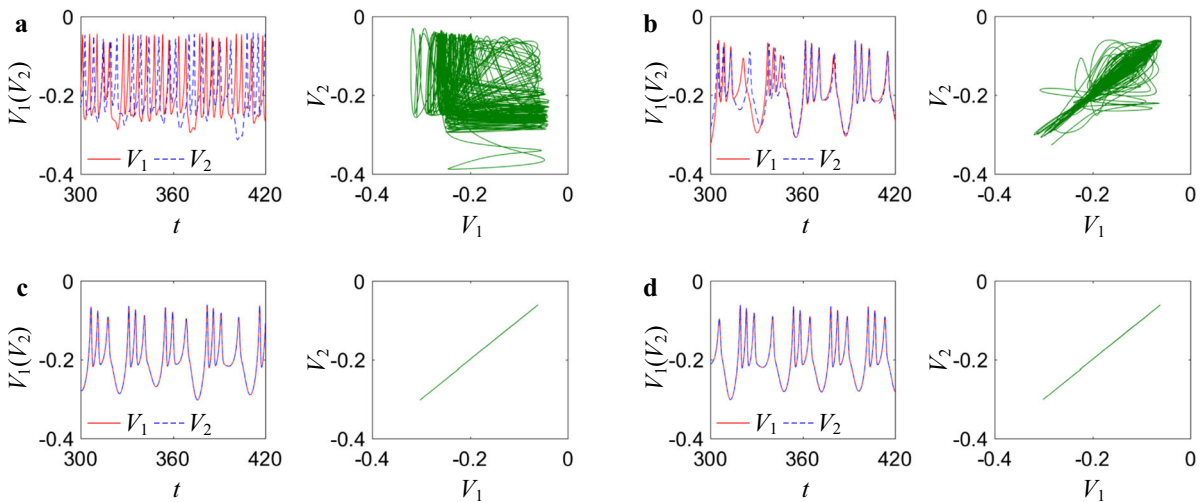


Fig. 6 Synchronous firing activities of the homogeneous memristive bi-neuron network with different induction coefficient k and memristor initial value φ_0 , where the lefts are time sequences of bursting behaviors, the rights are synchronization transition

states, the units of V_1, V_2 are mV, and the units of I_1, I_2 are μA
a $k = 0.2, \varphi_0 = 2$ mWb **b** $k = 0.2, \varphi_0 = -0.5$ mWb **c** $k = 0.2, \varphi_0 = -1$ mWb **d** $k = 0.4, \varphi_0 = -0.5$ mWb

When $\varphi_0 = 2$ mWb and -0.5 mWb with $k = 0.2$ are selected, there exist the relatively large errors between the two membrane potentials, indicating that the two coupling neurons are out of synchronization, as shown in Fig. 6a, b. However, when $k = 0.2, \varphi_0 = -1$ mWb as well as $k = 0.4, \varphi_0 = -0.5$ mWb are selected, the state of two coupling neurons is asymptotically synchronized, as shown in Fig. 6c, d. Therefore, memristor synapse coupling can enhance the synchronization between the two coupling neurons, including the larger induction coefficient and more negative memristor initial value.

Memristor synapse coupling could be much more effective to propagate signals between adjacent neurons and implement information encoding for these neurons [1]. As shown in Fig. 6, with decreasing the memristor initial value φ_0 or increasing the induction coefficient k , the two coupling neurons can achieve asymptotical synchronization and the error between the two membrane potentials is decreased entirely. The underlying mechanism could be that memristor synapse coupling can exchange the magnetic flux and the induced current can be applied to actuate the neuron to keep in sync with another neuron. The weak electromagnetic induction effect outputs small induced current by memristor synapse, leading to that the two coupling neurons are out of synchronization.

Secondly, the induction coefficient is kept for fixed $k = 0.2$. Except for the changes in the slow bursting variable initial values I_{10} and I_{20} , all the initial values are zero. When six sets of the initial values I_{10} and I_{20} are assigned, the bursting behaviors and synchronization transition states are shown in Fig. 7, from which different synchronous activities can be observed in the homogeneous memristive bi-neuron network. The numerical results demonstrate that the synchronous activities are closely related to the bi-neuron initial values also.

Now synchronizability is explored by altering the values of the mixed parameter k and initial value φ_0 as well as the initial values I_{10} and I_{20} . To quantitatively depict the error of two action trajectories, a normalized mean synchronization error E can be utilized [35,51], which is defined as

$$E = \frac{1}{N} \sum_{n=1}^N \frac{\sqrt{[V_1(n) - V_2(n)]^2 + [W_1(n) - W_2(n)]^2 + [I_1(n) - I_2(n)]^2}}{\sqrt{V_1(n)^2 + W_1(n)^2 + I_1(n)^2 + V_2(n)^2 + W_2(n)^2 + I_2(n)^2}} \tag{14}$$

where $V_j(n), W_j(n)$, and $I_j(n)$ are the n th sampling values with N samples during a time sequence interval. With (14), the normalized mean synchronization error of the homogeneous memristive bi-neuron network can be calculated, so that $E \rightarrow 0$ is relative to the synchronous state.

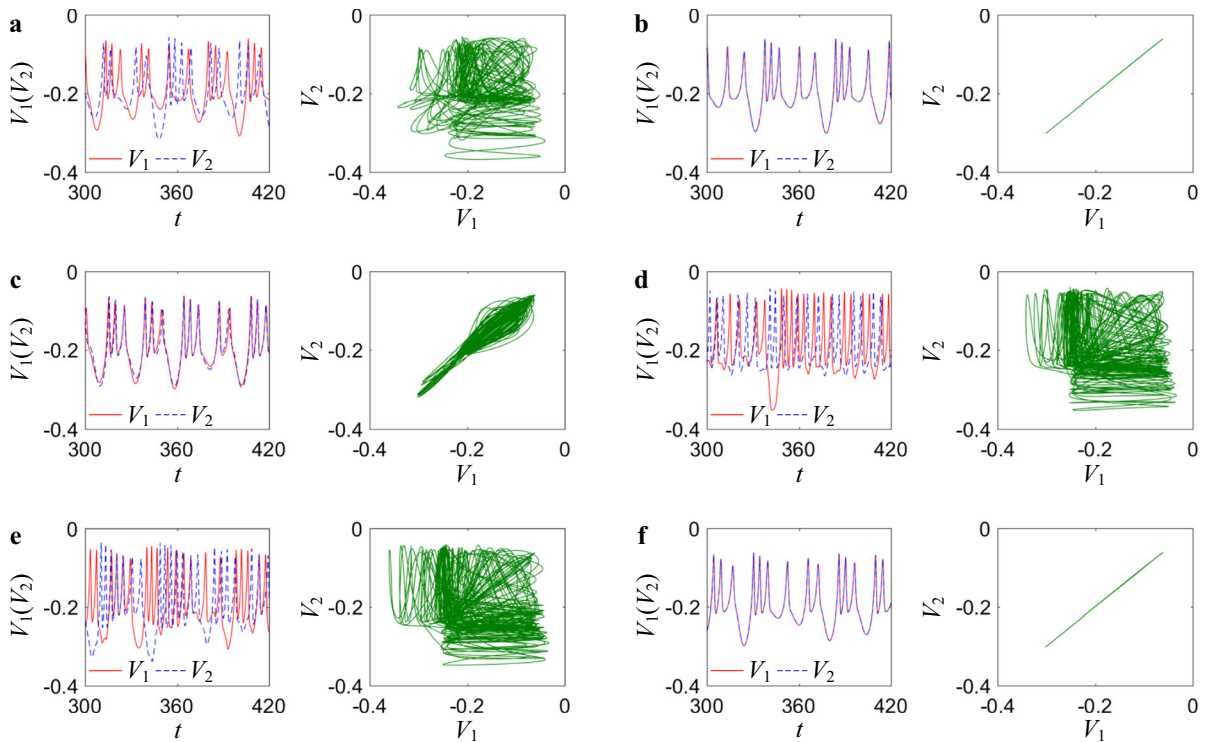


Fig. 7 Synchronous activities of the homogeneous memristive bi-neuron network with different initial values I_{10} and I_{20} , where $k = 0.2$, all other initial values are zero, the lefts are time sequences of bursting behaviors, and the rights are synchroniza-

tion transition states, the units of V_1, V_2 are mV, and the units of I_1, I_2 are μA **a** $I_{10} = 0, I_{20} = 0$ **b** $I_{10} = 0.1 \mu\text{A}, I_{20} = 0$ **c** $I_{10} = 0.05 \mu\text{A}, I_{20} = 0$ **d** $I_{10} = -0.1 \mu\text{A}, I_{20} = 0$ **e** $I_{10} = 0, I_{20} = 0.1 \mu\text{A}$ **f** $I_{10} = 0, I_{20} = -0.1 \mu\text{A}$

For the time sequence interval $[500, 600]$ with the time-step 0.01 and sample size $N = 10000$, the normalized mean synchronization error for different induction coefficient k and memristor initial value φ_0 is plotted in the $\varphi_0 - k$ plane, as shown in Fig. 8a. The red region indicates the two coupling neurons in synchronization with E close to zero; however, the other color regions denote the two coupling neurons out of synchronization with E having positive values. By increasing the induction coefficient k , the normalized mean synchronization error E drops near zero for more negative memristor initial value φ_0 , following that the two coupling neurons become synchronizable. Meanwhile, when the memristor initial value φ_0 is of a small negative value or a positive value, the two neurons are asynchronous for all values of the induction coefficient k .

Similarly, the normalized mean synchronization error for different slow bursting variable initial values I_{10} and I_{20} is drawn in the $I_{10} - I_{20}$ plane, as shown in Fig. 8b. The boundary between the synchronization

and asynchronization locates just below the diagonal line, in which the bottom right area colored by the red represents the two coupling neurons in synchronization with E close to zero; oppositely, the top left area colored by the black represents the two coupling neurons out of synchronization with E positive values. Particularly, only a narrow transition area appears in Fig. 8b, different from that in Fig. 8a, which demonstrates that the synchronous firing activities are extremely sensitive to the initial values of two neuron membrane potentials in the homogeneous memristive bi-neuron network.

From the normalized mean synchronized errors given in Fig. 8, it is concluded that the synchronous firing activities in the homogeneous memristive bi-neuron network are associated with the induction coefficient, and specially the initial values of memristor synapse and coupling neurons. Such the synchronous firing activities closely related to the initial values have not been reported yet in the previously published achievements.

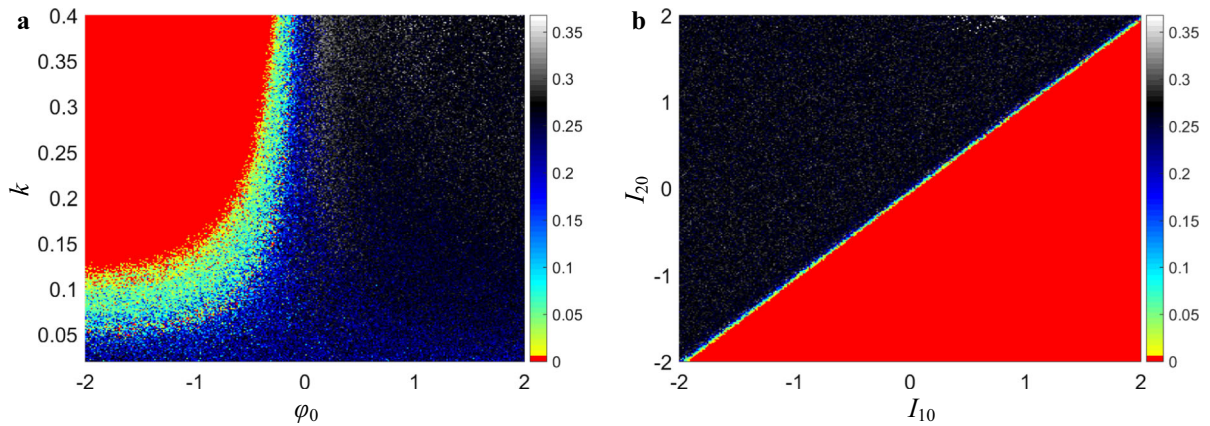


Fig. 8 Normalized mean synchronized errors of the homogeneous memristive bi-neuron network in the $\varphi_0 - k$ plane and the $I_{10} - I_{20}$ plane, where the unit of φ_0 is mWb and the units of

I_{10}, I_{20} are μA **a** for different induction coefficient k and memristor initial value φ_0 **b** for different slow bursting variable initial values I_{10} and I_{20}

5 FPGA-based experimental confirmation

To show the physical implementation of the proposed memristive bi-neuron network, a digitally circuit-implemented electronic bi-neuron network is designed using FPGA [52,53], based on which the initial-induced coexisting and synchronous firing activities of biological process in the memristive bi-neuron network can be observed experimentally.

A Xilinx FPGA (Zynq xc7z020) board with extended interfaces is employed to implement the proposed memristor synapse-coupled Morris–Lecar bi-neuron network. The register transfer level (RTL) schematic diagram of the digitally circuit-implemented electronic bi-neuron network is depicted, as shown in Fig. 9. Floating-point operation IP cores are called to construct Verilog HDL programs in Vivado integrated development environment (IDE). To guarantee high computation accuracy, pure floating-point operations are applied on FPGA without using bit shifting for fixed-point multiplication and any approximations such as piecewise linearization [52,53]. The verilog HDL programs are optimized to reduce the resource utilization by carefully designing time multiplexing sequence. For instance, the modules using for computations of $(M_{\infty 1}, W_{\infty 1}, \tau_{\infty 1})$ and $(M_{\infty 2}, W_{\infty 2}, \tau_{\infty 2})$ have the same function with two different input variables V_1 and V_2 such that only one module of $(M_{\infty j}, W_{\infty j}, \tau_{\infty j})$ is instanced and called to attain the results of $(M_{\infty 1}, W_{\infty 1}, \tau_{\infty 1})$ and $(M_{\infty 2}, W_{\infty 2}, \tau_{\infty 2})$ in order. Two selected floating-

point variables are transformed into integer-type numbers before being sent to a two-channel DAC (AD9767) board which is installed on the FPGA extended interface. The two analog signals converted by the DAC board are measured in the XY displaying mode or normal mode on a Keysight DSO-X 4154A oscilloscope.

To demonstrate the FPGA-based digital experimental results, the heterogeneous memristive bi-neuron network is considered. The parameters and initial values of two coupling neurons along with the memristor induction coefficient are assigned as those used in Fig. 4. Corresponding to the numerical results given in Fig. 4, the experimentally captured results for different values of memristor initial value φ_0 are provided, as shown in Fig. 10, where for each memristor initial value, the phase plots of two coupling neurons and time sequences of two membrane potentials are overlapped on each picture by post-processing. One thing to note is that for the digitally circuit-implemented electronic bi-neuron network, all the parameters are dimensionless and have no physical meaning. Therefore, complex memristor initial-induced coexisting firing activities can be experimentally observed in such a memristive bi-neuron network. Generally ignoring the errors in amplitudes caused by same linear scaling, the experimental results in Fig. 10 well match with the numerical simulations in Fig. 4, indicating the feasibility of the digitally circuit-implemented electronic bi-neuron network. Analo-

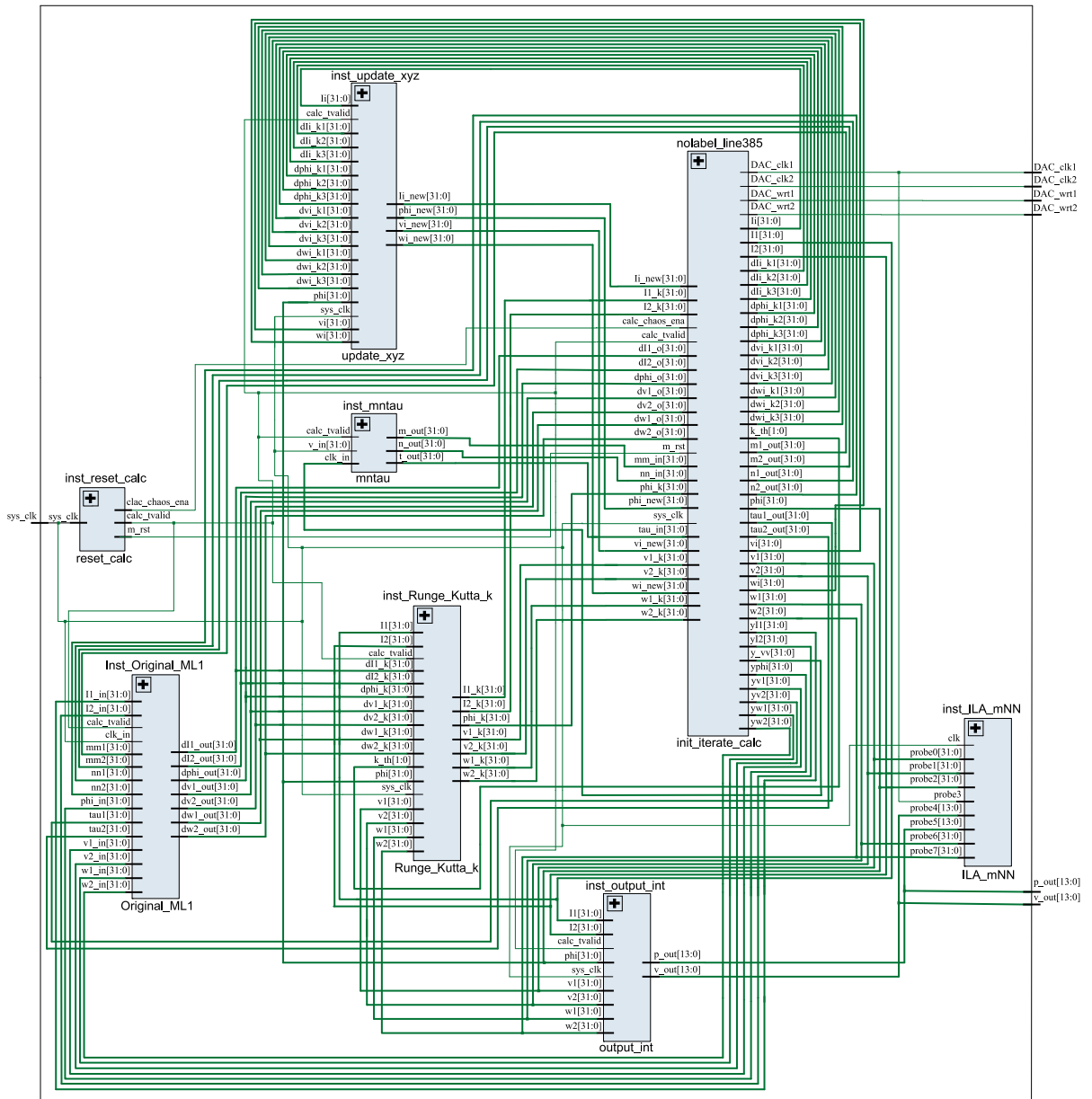


Fig. 9 RTL schematic diagram of the memristor synapse-coupled Morris–Lecar bi-neuron network implemented in Zynq xc7z020 FPGA board

gously, the aforementioned numerical synchronous firing activities in the homogeneous memristive bi-neuron network can be also captured in the digitally circuit-implemented electronic bi-neuron network, which are omitted here.

6 Conclusions

A memristor synapse-coupled bi-neuron network was presented, which was completed by bidirectionally coupling two three-dimensional heterogeneous or homogeneous Morris–Lecar neurons with a memristor synapse. Due to the existence of a line equilibrium set, coexisting firing activities in the heteroge-

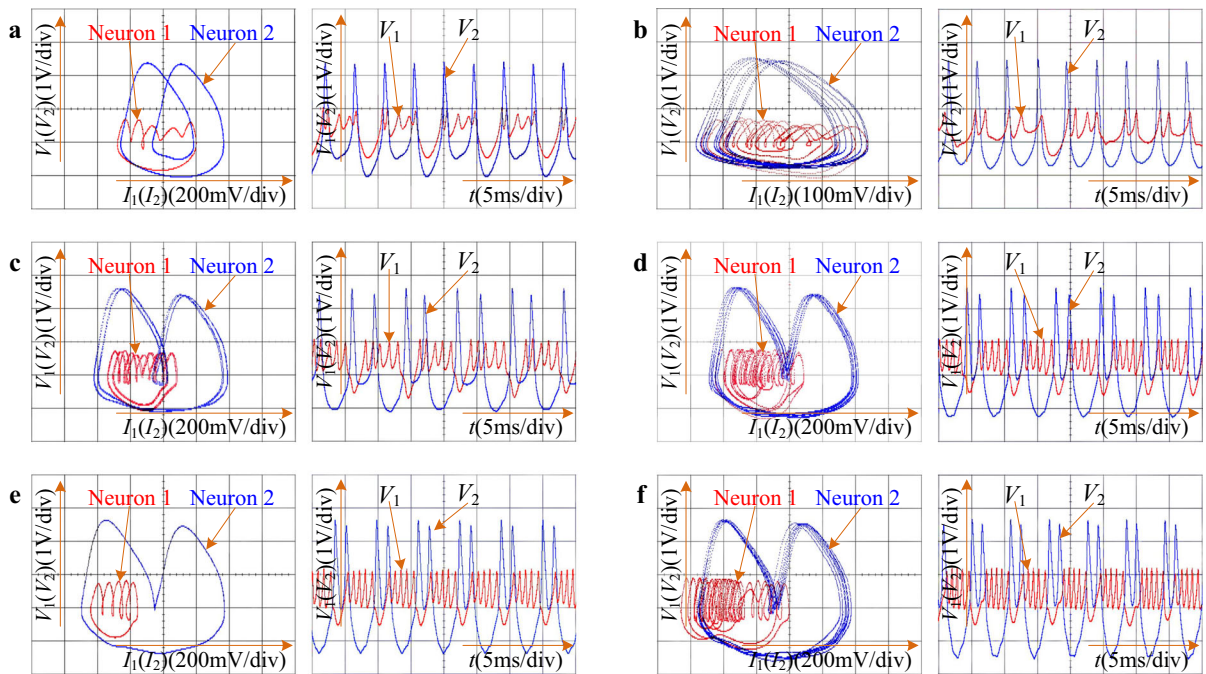


Fig. 10 FPGA-based experimentally captured results of memristor initial-induced infinitely many coexisting patterns for $k = 0.2$, the lefts are phase plots of neuron 1 in the $I_1 - V_1$ plane and neuron 2 in the $I_2 - V_2$ plane, the rights are time sequences of the membrane potentials V_1 and V_2 **a** periodic burster-5 bursting and periodic tonic-spiking for $\varphi_0 = -1$ **b** hyperchaotic bursting and

hyperchaotic tonic-spiking for $\varphi_0 = -0.15$ **c** periodic bursting with quadruple burster-5 and periodic tonic-spiking for $\varphi_0 = 0.45$ **d** chaotic bursting and chaotic tonic-spiking for $\varphi_0 = 1$ **e** another periodic burster-5 bursting and periodic tonic-spiking for $\varphi_0 = 1.5$ **f** hyperchaotic bursting and hyperchaotic tonic-spiking for $\varphi_0 = 3$

neous memristive bi-neuron network were explored, upon which initial-induced infinitely many firing patterns with extreme multistability were numerically disclosed. Meanwhile, synchronous firing activities in the homogeneous memristive bi-neuron network were investigated. It can be found theoretically and numerically that the two coupling neurons are easier to completely synchronize for more negative memristor initial value along with larger induction coefficient, but their synchronous firing activities can be affected by the initial values of two coupling neurons. Furthermore, a digitally circuit-implemented electronic bi-neuron network was designed using FPGA and the memristor initial-induced coexisting firing activities were captured to experimentally confirm the numerical plots. The investigations for memristor synapse-coupled bi-neuron network can provide some new insights for understanding the actual firing activities of neuron-based complex network. Moreover, when a multiplayer or chain neural network is modeled by the Morris-Lecar neurons, what kinds of the collective behaviors,

for example, chimera state [54], will be encountered in the network involved field coupling, or/and noise, or/and chemical autapse [55,56], which could be considered for future research issues.

Acknowledgements This work was supported by the Grants from the National Natural Science Foundations of China under 51777016, 61801054, and 61601062, and the Natural Science Foundation of Jiangsu Province, China, under Grant No. BK20191451.

Compliance with ethical standards

Conflict of interest The authors declare that they have no conflict of interest.

References

1. Ma, J., Tang, J.: A review for dynamics of collective behaviors of network of neurons. *Sci. China Technol. Sci* **58**, 2038–2045 (2015)
2. Wu, J., Xu, Y., Ma, J.: Lévy noise improves the electrical activity in a neuron under electromagnetic radiation. *PLoS ONE* **12**, e0174330 (2017)

3. Parastesh, F., Rajagopal, K., Karthikeyan, A., Alsaedi, A., Hayat, T., Pham, V.-T.: Complex dynamics of a neuron model with discontinuous magnetic induction and exposed to external radiation. *Cognit. Neurodyn.* **12**, 607–614 (2018)
4. Lv, M., Wang, C., Ren, G., Ma, J., Song, X.: Model of electrical activity in a neuron under magnetic flow effect. *Nonlinear Dyn.* **85**, 1479–1490 (2016)
5. Wang, Y., Ma, J., Xu, Y., Wu, F., Zhou, P.: The electrical activity of neurons subject to electromagnetic induction and Gaussian white noise. *Int. J. Bifurc. Chaos* **27**, 1750030 (2017)
6. Wu, F., Wang, C., Jin, W., Ma, J.: Dynamical responses in a new neuron model subjected to electromagnetic induction and phase noise. *Physica A* **469**, 81–88 (2017)
7. Xu, Y., Jia, Y., Ma, J., Alsaedi, A., Ahmad, B.: Synchronization between neurons coupled by memristor. *Chaos Soliton Fract.* **104**, 435–442 (2017)
8. Ma, J., Lv, M., Zhou, P., Xu, Y., Hayat, T.: Phase synchronization between two neurons induced by coupling of electromagnetic field. *Appl. Math. Comput.* **307**, 321–328 (2017)
9. Ren, G., Xu, Y., Wang, C.: Synchronization behavior of coupled neuron circuits composed of memristors. *Nonlinear Dyn.* **88**, 893–901 (2017)
10. Xu, F., Zhang, J., Fang, T., Huang, S., Wang, M.: Synchronous dynamics in neural system coupled with memristive synapse. *Nonlinear Dyn.* **92**, 1395–1402 (2018)
11. Ge, M., Jia, Y., Xu, Y., Yang, L.: Mode transition in electrical activities of neuron driven by high and low frequency stimulus in the presence of electromagnetic induction and radiation. *Nonlinear Dyn.* **91**, 515–523 (2018)
12. Lu, L., Jia, Y., Liu, W., Yang, L.: Mixed stimulus-induced mode selection in neural activity driven by high and low frequency current under electromagnetic radiation. *Complexity* **2017**, 7628537 (2017)
13. Lv, M., Ma, J.: Multiple modes of electrical activities in a new neuron model under electromagnetic radiation. *Neurocomputing* **205**, 375–381 (2016)
14. Wu, J., Ma, S.: Coherence resonance of the spiking regularity in a neuron under electromagnetic radiation. *Nonlinear Dyn.* **96**, 1895–1908 (2019)
15. Bao, B., Hu, A., Bao, H., Xu, Q., Chen, M., Wu, H.: Three-dimensional memristive Hindmarsh–Rose neuron model with hidden coexisting asymmetric behaviors. *Complexity* **2018**, 3872573 (2018)
16. Bao, H., Hu, A., Liu, W., Bao, B.: Hidden bursting firings and bifurcation mechanisms in memristive neuron model with threshold electromagnetic induction. *IEEE Trans. Neural Netw. Learn. Syst.* (2019). <https://doi.org/10.1109/TNNLS.2019>
17. Bao, H., Liu, W., Hu, A.: Coexisting multiple firing patterns in two adjacent neurons coupled by memristive electromagnetic induction. *Nonlinear Dyn.* **95**, 43–56 (2019)
18. Bennett, D.J., Li, Y., Harvey, P.J., Gorassini, M.: Evidence for plateau potentials in tail motoneurons of awake chronic spinal rats with spasticity. *J. Neurophysiol.* **86**, 1972–1982 (2001)
19. Kim, H., Jones, K.E.: Asymmetric electrotonic coupling between the soma and dendrites alters the bistable firing behaviour of reduced models. *J. Comput. Neurosci.* **30**, 659–674 (2011)
20. Bao, B., Hu, A., Xu, Q., Bao, H., Wu, H., Chen, M.: AC induced coexisting asymmetric bursters in the improved Hindmarsh–Rose model. *Nonlinear Dyn.* **92**, 1695–1706 (2018)
21. Bao, B., Yang, Q., Zhu, L., Bao, H., Xu, Q., Yu, Y., Chen, M.: Chaotic bursting dynamics and coexisting multi-stable firing patterns in 3D autonomous M–L model and microcontroller-based validations. *Int. J. Bifurc. Chaos* **29**, 1950134 (2019)
22. Pisarchik, A.N., Jaimes-Reátegui, R., García-Vellisca, M.A.: Asymmetry in electrical coupling between neurons alters multistable firing behavior. *Chaos* **28**, 033605 (2018)
23. Bao, H., Liu, W., Chen, M.: Hidden extreme multistability and dimensionality reduction analysis for an improved non-autonomous memristive FitzHugh–Nagumo circuit. *Nonlinear Dyn.* **96**, 1879–1894 (2019)
24. Fozin, F.T., Kengne, J., Pelap, F.B.: Dynamical analysis and multistability in autonomous hyperchaotic oscillator with experimental verification. *Nonlinear Dyn.* **93**, 653–669 (2018)
25. Pisarchik, A.N., Feudel, U.: Control of multistability. *Phys. Rep.* **540**, 167–218 (2014)
26. Chen, M., Sun, M., Bao, H., Hu, Y., Bao, B.: Flux-charge analysis of two-memristor-based Chua’s circuit: dimensionality decreasing model for detecting extreme multistability. *IEEE Trans. Ind. Electron.* **67**, 2197–2206 (2020)
27. Sun, H., Scott, S.K., Showalter, K.: Uncertain destination dynamics. *Phys. Rev. E* **60**, 3876–3880 (1999)
28. Patel, M.S., Patel, U., Sen, A., Sethia, G.C., Hens, C., Dana, S.K., Feudel, U., Showalter, K., Ngonghala, C.N., Amritkar, R.E.: Experimental observation of extreme multistability in an electronic system of two coupled Rössler oscillators. *Phys. Rev. E* **89**, 022918 (2014)
29. Zhang, Y., Liu, Z., Wu, H., Chen, S., Bao, B.: Dimensionality reduction analysis for detecting initial effects on synchronization of memristor-coupled system. *IEEE Access* **7**, 109689–109698 (2019)
30. Usha, K., Subha, P.: Energy feedback and synchronous dynamics of Hindmarsh–Rose neuron model with memristor. *Chin. Phys. B* **28**, 02050 (2019)
31. Parastesh, F., Rajagopal, K., Alsaedi, F.E., Hayat, T., Pham, V.-T., Hussain, I.: Birth and death of spiral waves in a network of Hindmarsh–Rose neurons with exponential magnetic flux and excitable media. *Appl. Math. Comput.* **354**, 377–384 (2019)
32. Soriano, D.C., Santos, O.V.D., Suyama, R., Fazanaro, F.I., Attux, R.: Conditional Lyapunov exponents and transfer entropy in coupled bursting neurons under excitation and coupling mismatch. *Commun. Nonlinear Sci. Numer. Simul.* **56**, 419–433 (2018)
33. Wu, K., Wang, T., Wang, C., Du, T., Lu, H.: Study on electrical synapse coupling synchronization of Hindmarsh–Rose neurons under Gaussian white noise. *Neural Comput. Appl.* **30**, 551–561 (2018)
34. Mostaghimi, S., Nazarimehr, F., Jafari, S., Ma, J.: Chemical and electrical synapse-modulated dynamical properties of coupled neurons under magnetic flow. *Appl. Math. Comput.* **348**, 42–56 (2019)
35. Parastesh, F., Azarnoush, H., Jafari, S., Hatf, B., Perc, M., Repnik, R.: Synchronizability of two neurons with switching in the coupling. *Appl. Math. Comput.* **350**, 217–223 (2019)

36. Ge, M., Jia, Y., Kirunda, J., Xu, Y., Shen, J., Lu, L., Liu, Y., Pei, Q., Zhan, X., Yang, L.: Propagation of firing rate by synchronization in a feed-forward multilayer Hindmarsh-Rose neural network. *Neurocomputing* **320**, 60–68 (2018)
37. Eckhorn, R.: Neural mechanisms of scene segmentation: recording from the visual cortex suggest basic circuits or linking field models. *IEEE Trans. Neural Netw.* **10**, 464–479 (1999)
38. Bartsch, R., Kantelhardt, J.W., Penzel, T., Havlin, S.: Experimental evidence for phase synchronization transitions in the human cardiorespiratory system. *Phys. Rev. Lett.* **98**, 54102 (2007)
39. Uhlhaas, P.J., Singer, W.: Neural synchrony in brain disorders: relevance for cognitive dysfunctions and pathophysiology. *Neuron* **52**, 155–168 (2006)
40. Xu, Y., Jia, Y., Wang, H., Liu, Y., Wang, P., Zhao, Y.: Spiking activities in chain neural network driven by channel noise with field coupling. *Nonlinear Dyn.* **95**, 3237–3247 (2019)
41. Pinto, R.D., Varona, P., Volkovskii, A.R., Szücs, A., Abarbanel, H.D., Rabinovich, M.I.: Synchronous behavior of two coupled electronic neurons. *Phys. Rev. E* **62**, 2644–2656 (2000)
42. Linaro, D., Poggi, T., Storace, M.: Experimental bifurcation diagram of a circuit-implemented neuron model. *Phys. Lett. A* **374**, 4589–4593 (2011)
43. Dahasert, N., Öztürk, I., Kiliç, R.: Experimental realizations of the HR neuron model with programmable hardware and synchronization applications. *Nonlinear Dyn.* **70**, 2343–2358 (2012)
44. Bilotta, E., Pantano, P., Vena, S.: Speeding up cellular neural network processing ability by embodying memristors. *IEEE Trans. Neural Netw. Learn. Syst.* **28**, 1228–1232 (2017)
45. Izhikevich, E.M.: Neural excitability, spiking and bursting. *Int. J. Bifurc. Chaos* **10**, 1171–1266 (2000)
46. Rajamani, V., Kim, H., Chua, L.O.: Morris–Lecar model of third-order barnacle muscle fiber is made of volatile memristors. *Sci. China Inf. Sci.* **61**, 060426 (2018)
47. Shi, M., Wang, Z.: Abundant bursting patterns of a fractional-order Morris–Lecar neuron model. *Commun. Nonlinear Sci. Numer. Simulat.* **19**, 1956–1969 (2014)
48. Chen, C., Chen, J., Bao, H., Chen, M., Bao, B.: Coexisting multi-stable patterns in memristor synapse-coupled Hopfield neural network with two neurons. *Nonlinear Dyn.* **95**, 3385–3399 (2019)
49. Khalil, H.K.: *Nonlinear Systems*, 3rd edn. Prentice-Hall, Upper Saddle River (2002)
50. Liu, Y., Ren, G., Zhou, P., Hayat, T., Ma, J.: Synchronization in networks of initially independent dynamical systems. *Phys. A* **520**, 370–380 (2019)
51. Buscarino, A., Frasca, M., Branciforte, M., Fortuna, L., Sprott, J.C.: Synchronization of two Rössler systems with switching coupling. *Nonlinear Dyn.* **88**, 673–683 (2017)
52. Hayati, M., Nouri, M., Haghiri, S., Abbott, D.: Digital multiplierless realization of two coupled biological Morris–Lecar neuron model. *IEEE Trans. Circuits Syst. I Reg. Pap.* **62**, 1805–1814 (2015)
53. Hua, Z., Zhou, B., Zhou, Y.: Sine chaotification model for enhancing chaos and its hardware implementation. *IEEE Trans. Ind. Electron.* **66**, 1273–1284 (2018)
54. Rakshit, S., Bera, B.K., Perc, M., Ghosh, D.: Basin stability for chimera states. *Sci. Rep.* **7**, 2412 (2017)
55. Lu, L., Jia, Y., Kirunda, J., Xu, Y., Ge, M., Pei, Q., Yang, L.: Effects of noise and synaptic weight on propagation of sub-threshold excitatory postsynaptic current signal in a feed-forward neural network. *Nonlinear Dyn.* **95**, 1673–1686 (2019)
56. Ge, M., Jia, Y., Xu, Y., Lu, L., Wang, H., Zhao, Y.: Wave propagation and synchronization induced by chemical autapse in chain Hindmarsh–Rose neural network. *Appl. Math. Comput.* **352**, 136–145 (2019)

Publisher's Note Springer Nature remains neutral with regard to jurisdictional claims in published maps and institutional affiliations.